Measurement of double-spin asymmetries associated with deeply virtual Compton scattering on a transversely polarized hydrogen target

HERMES Collaboration

A. Airapetian [l,o], N. Akopov [z], Z. Akopov [e], E.C. Aschenauer [f,1], W. Augustyniak [y], R. Avakian [z], A. Avetissian [z], E. Avetisyan [e], S. Belostotski [r], N. Bianchi [j], H.P. Blok [q,x], A. Borissov [e], J. Bowles [m], I. Brodski [l], V. Bryzgalov [s], J. Burns [m], M. Capiluppi [i], G.P. Capitani [j], E. Cisbani [u], G. Ciullo [i], M. Contalbrigo [i], P.F. Dalpiaz [i], W. Deconinck [e], R. De Leo [b], L. De Nardo [k,e], E. De Sanctis [j], P. Di Nezza [j], M. Düren [l], M. Ehrenfried [l], G. Elbakian [z], F. Ellinghaus [d], R. Fabbri [f], A. Fantoni [j], L. Felawka [v], S. Frullani [u], D. Gabbert [f], G. Gapienko [s], V. Gapienko [s], F. Garibaldi [u], G. Gavrilov [e,r,v], V. Gharibyan [z], F. Giordano [e,i], S. Gliske [a,o], M. Golembiovskaya [f], M. Hartig [e], D. Hasch [j], M. Hoek [m], Y. Holler [e], I. Hristova [f], Y. Imazu [w], A. Ivanilov [s], H.E. Jackson [a], H.S. Jo [k], S. Joosten [n], R. Kaiser [m,2], G. Karyan [z], T. Keri [m,l], E. Kinney [d], A. Kisselev [r], V. Korotkov [s], V. Kozlov [p], P. Kravchenko [h,r], V.G. Krivokhijine [g], L. Lagamba [b], L. Lapikás [q], I. Lehmann [m], P. Lenisa [i], A. López Ruiz [k], W. Lorenzon [o], X.-G. Lu [e], X.-R. Lu [w], B.-Q. Ma [c], D. Mahon [m], N.C.R. Makins [n], S.I. Manaenkov [r], L. Manfré [u], Y. Mao [c], B. Marianski [y], A. Martinez de la Ossa [e,d], H. Marukyan [z], C.A. Miller [v], Y. Miyachi [w,3], A. Movsisyan [z], M. Murray [m], A. Mussgiller [e,h], E. Nappi [b], Y. Naryshkin [r], A. Nass [h], M. Negodaev [f], W.-D. Nowak [f], L.L. Pappalardo [i], R. Perez-Benito [l], M. Raithel [h], P.E. Reimer [a], A.R. Reolon [j], C. Riedl [f], K. Rith [h,*], G. Rosner [m], A. Rostomyan [e], J. Rubin [a,n], D. Ryckbosch [k], Y. Salomatin [s], A. Schäfer [t], G. Schnell [f,k,4], K.P. Schüler [e], B. Seitz [m], T.-A. Shibata [w], V. Shutov [g], M. Stancari [i], M. Statera [i], E. Steffens [h], J.J.M. Steijger [q], F. Stinzing [h], S. Taroian [z], A. Terkulov [p], R. Truty [n], A. Trzcinski [y], M. Tytgat [k], Y. Van Haarlem [k], C. Van Hulse [k], D. Veretennikov [r], V. Vikhrov [r], I. Vilardi [b], S. Wang [c], S. Yaschenko [f,h], Z. Ye [e], S. Yen [v], V. Zagrebelnyy [l,e], D. Zeiler [h], B. Zihlmann [e], P. Zupranski [y]

[a] *Physics Division, Argonne National Laboratory, Argonne, IL 60439-4843, USA*
[b] *Istituto Nazionale di Fisica Nucleare, Sezione di Bari, 70124 Bari, Italy*
[c] *School of Physics, Peking University, Beijing 100871, China*
[d] *Nuclear Physics Laboratory, University of Colorado, Boulder, CO 80309-0390, USA*
[e] *DESY, 22603 Hamburg, Germany*
[f] *DESY, 15738 Zeuthen, Germany*
[g] *Joint Institute for Nuclear Research, 141980 Dubna, Russia*
[h] *Physikalisches Institut, Universität Erlangen-Nürnberg, 91058 Erlangen, Germany*
[i] *Istituto Nazionale di Fisica Nucleare, Sezione di Ferrara and Dipartimento di Fisica, Università di Ferrara, 44100 Ferrara, Italy*
[j] *Istituto Nazionale di Fisica Nucleare, Laboratori Nazionali di Frascati, 00044 Frascati, Italy*
[k] *Department of Subatomic and Radiation Physics, University of Gent, 9000 Gent, Belgium*
[l] *Physikalisches Institut, Universität Gießen, 35392 Gießen, Germany*
[m] *SUPA, School of Physics and Astronomy, University of Glasgow, Glasgow G12 8QQ, United Kingdom*
[n] *Department of Physics, University of Illinois, Urbana, IL 61801-3080, USA*
[o] *Randall Laboratory of Physics, University of Michigan, Ann Arbor, MI 48109-1040, USA*
[p] *Lebedev Physical Institute, 117924 Moscow, Russia*
[q] *National Institute for Subatomic Physics (Nikhef), 1009 DB Amsterdam, The Netherlands*
[r] *Petersburg Nuclear Physics Institute, Gatchina, Leningrad region 188300, Russia*
[s] *Institute for High Energy Physics, Protvino, Moscow region 142281, Russia*
[t] *Institut für Theoretische Physik, Universität Regensburg, 93040 Regensburg, Germany*
[u] *Istituto Nazionale di Fisica Nucleare, Sezione di Roma, gruppo Sanità and Istituto Superiore di Sanità, 00161 Rome, Italy*
[v] *TRIUMF, Vancouver, British Columbia V6T 2A3, Canada*
[w] *Department of Physics, Tokyo Institute of Technology, Tokyo 152, Japan*
[x] *Department of Physics and Astronomy, VU University, 1081 HV Amsterdam, The Netherlands*
[y] *Andrzej Soltan Institute for Nuclear Studies, 00-689 Warsaw, Poland*
[z] *Yerevan Physics Institute, 375036 Yerevan, Armenia*

A B S T R A C T

Double-spin asymmetries in exclusive electroproduction of real photons from a transversely polarized hydrogen target are measured with respect to the product of target polarization with beam helicity and beam charge, and with respect to the product of target polarization with beam helicity alone. The asymmetries arise from the deeply virtual Compton scattering process and its interference with the Bethe–Heitler process. They are related to the real part of the same combination of Compton form factors as that determining the previously published transverse target single-spin asymmetries through the imaginary part. The results for the double-spin asymmetries are found to be compatible with zero within the uncertainties of the measurement, and are not incompatible with the predictions of the only available GPD-based calculation.

1. Introduction

Generalized Parton Distributions (GPDs) provide a framework for describing the multidimensional structure of the nucleon [1–3]. They encompass information on the correlated transverse spatial and longitudinal momentum distributions of partons in the nucleon [4–9]. Furthermore, access to the parton total angular momentum contribution to the nucleon spin may be provided by GPDs through the Ji relation [3].

Hard exclusive leptoproduction of a meson or photon, leaving only an intact nucleon in the final state, can be described in terms of GPDs. GPDs depend on four kinematic variables: t, x, ξ, and Q^2. The Mandelstam variable $t = (p - p')^2$ is the squared four-momentum transfer to the target nucleon, with p (p') its initial (final) four-momentum. In the 'infinite'-target-momentum frame, x and ξ are related to the longitudinal momentum of the struck parton, as a fraction of the target momentum. The variable x is the average of the initial and final momentum fractions carried by the parton, and the variable ξ, known as the skewness, is half of their difference. The evolution of GPDs with $Q^2 \equiv -q^2$, where $q = k - k'$ is the difference between the four-momenta of the incident and scattered leptons, can be calculated in the context of perturbative quantum chromodynamics as in the case of parton distribution functions. This evolution has been evaluated to leading order [1–3,10] and next-to-leading order [11–13] in the strong coupling constant α_s. The skewness ξ can be related to the Bjorken scaling variable $x_B \equiv Q^2/(2p \cdot q)$ through $\xi \simeq x_B/(2 - x_B)$ in the generalized Bjorken limit of large Q^2, and fixed x_B and t. There is currently no consensus about how to define ξ in terms of experimental observables; hence the experimental results are typically reported as projections in x_B. The entire x dependences of GPDs are generally not yet experimentally accessible, an exception being the trajectory $x = \xi$ [14,15].

The description of a spin-1/2 hadron such as the nucleon includes four leading-twist quark-chirality-conserving GPDs H, E, $\widetilde{H}$, and $\widetilde{E}$ [1–3,16]. The GPDs H and E are quark-helicity averaged, whereas $\widetilde{H}$ and $\widetilde{E}$ are related to quark-helicity differences. The GPDs H and $\widetilde{H}$ conserve nucleon helicity, while E and $\widetilde{E}$ are associated with a helicity flip of the nucleon. GPDs can be constrained through measurements of cross sections and asymmetries in ex-

clusive processes such as exclusive photon or meson production. In the case of photon production, the asymmetries arise from the Deeply Virtual Compton Scattering (DVCS) process, i.e., the hard exclusive leptoproduction of a real photon, where the photon is radiated by the struck quark, and its interference with the Bethe–Heitler (BH) process, where the photon is radiated by the initial- or final-state lepton. The DVCS process is currently the simplest experimentally accessible hard exclusive process that can be used to constrain GPDs, but only on the trajectory $x = \xi$.

A variety of results from DVCS measurements at DESY and Jefferson Laboratory was published in the last few years. This includes results on beam-helicity and beam-charge asymmetries from CLAS [17–19] and HERMES [20–22] as well as cross section measurements in Hall-A [23], all of which can serve to constrain mainly GPD H. HERMES additionally obtained results on transverse-target asymmetries [24], which can constrain GPD E. Knowledge on both H and E opens access towards the determination of the total u and d-quark angular momentum through the Ji sum rule [3]. This Letter reports the first measurement of azimuthal asymmetries with respect to target polarization combined with beam helicity and beam charge, and with respect to target polarization combined with beam helicity alone, for exclusive electroproduction of real photons from a transversely polarized hydrogen target. One of these new asymmetries also has the potential in principle to constrain GPD E.

2. Deeply virtual Compton scattering

2.1. Scattering amplitudes

The five-fold differential cross section for the leptoproduction of real photons from a transversely polarized hydrogen target reads [16]

$$\frac{d^5\sigma}{dx_B \, dQ^2 \, d|t| \, d\phi \, d\phi_S} = \frac{x_B \, e^6}{32(2\pi)^4 Q^4} \frac{|\mathcal{T}|^2}{\sqrt{1 + \varepsilon^2}}. \tag{1}$$

Here, e is the elementary charge, $\varepsilon \equiv 2x_B M_p/\sqrt{Q^2}$, where M_p is the mass of the proton, and $\mathcal{T}$ is the reaction amplitude. Two azimuthal angles ϕ and ϕ_S appear in the cross section in the case of transverse polarization of the target, and are defined in Fig. 1.

The initial and final states of the DVCS process are indistinguishable from those of the BH process. Hence the cross section contains the coherent superposition of the BH and DVCS amplitudes:

$$|\mathcal{T}|^2 = |\mathcal{T}_{BH} + \mathcal{T}_{DVCS}|^2$$
$$= |\mathcal{T}_{BH}|^2 + |\mathcal{T}_{DVCS}|^2 + \underbrace{\mathcal{T}_{DVCS}\mathcal{T}_{BH}^* + \mathcal{T}_{DVCS}^*\mathcal{T}_{BH}}_{I}, \tag{2}$$

* Corresponding author.
  E-mail address: klaus.rith@desy.de (K. Rith).
[1] Now at: Brookhaven National Laboratory, Upton, NY 11772-5000, USA.
[2] Present address: International Atomic Energy Agency, A-1400 Vienna, Austria.
[3] Now at: Department of Physics, Yamagata University, Yamagata 990-8560, Japan.
[4] Now at: Department of Theoretical Physics, University of the Basque Country UPV/EHU, 48080 Bilbao, Spain and IKERBASQUE, Basque Foundation for Science, 48011 Bilbao, Spain.
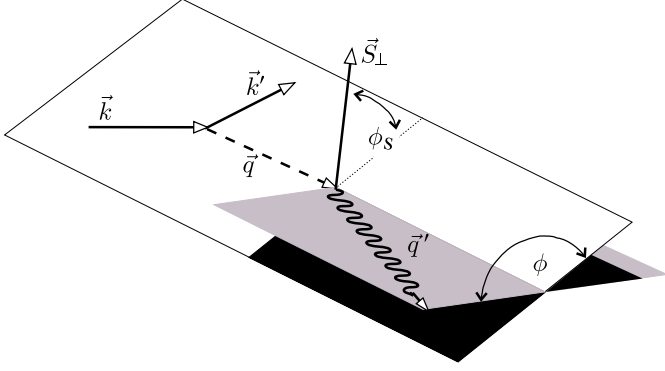
Fig. 1. Momenta and azimuthal angles for exclusive real-photon electroproduction in the target rest frame. The quantity ϕ denotes the angle between the lepton scattering plane containing the three-momenta $\vec{k}$ and $\vec{k}'$ of the incoming and outgoing lepton and the photon production plane correspondingly defined by the vector $\vec{q} = \vec{k} - \vec{k}'$ and the momentum $\vec{q}'$ of the real photon. The symbol ϕ_S denotes the angle between the lepton scattering plane and $\vec{S}_\perp$, the component of the target polarization vector that is orthogonal to $\vec{q}$. These definitions are consistent with the Trento conventions [25] and differ from those used in Ref. [16]: $\phi = \pi - \phi_{[16]}$ and $\phi - \phi_S = \pi + \varphi_{[16]}$.

where 'I' denotes the BH-DVCS interference term. The BH amplitude is calculable to leading order in QED using the form factors measured in elastic scattering. The interference term I and the squared DVCS amplitude $|\mathcal{T}_{\text{DVCS}}|^2$ in Eq. (2) provide experimental access to the (complex) DVCS amplitude through measurements of various cross section asymmetries [16].

Each of the three terms of Eq. (2) can be decomposed as a Fourier series:

$$|\mathcal{T}_{\text{BH}}|^2 = \frac{K_{\text{BH}}}{\mathcal{P}_1(\phi)\mathcal{P}_2(\phi)}\left\{\sum_{n=0}^{2} c_{n,\text{unp}}^{\text{BH}}\cos(n\phi)\right.$$
$$+ \lambda S_\perp\left[\sum_{n=0}^{1} c_{n,\text{TP}}^{\text{BH}}\cos(\phi-\phi_S)\cos(n\phi)\right.$$
$$\left.\left. + s_{1,\text{TP}}^{\text{BH}}\sin(\phi-\phi_S)\sin(\phi)\right]\right\}, \tag{3}$$

$$|\mathcal{T}_{\text{DVCS}}|^2 = K_{\text{DVCS}}\left\{\sum_{n=0}^{2} c_{n,\text{unp}}^{\text{DVCS}}\cos(n\phi) + \lambda s_{1,\text{unp}}^{\text{DVCS}}\sin(\phi)\right.$$
$$+ S_\perp\left[\sum_{n=0}^{2} c_{n,\text{TP}-}^{\text{DVCS}}\sin(\phi-\phi_S)\cos(n\phi)\right.$$
$$\left. + \sum_{n=1}^{2} s_{n,\text{TP}+}^{\text{DVCS}}\cos(\phi-\phi_S)\sin(n\phi)\right]$$
$$+ \lambda S_\perp\left[\sum_{n=0}^{1} c_{n,\text{TP}+}^{\text{DVCS}}\cos(\phi-\phi_S)\cos(n\phi)\right.$$
$$\left.\left. + s_{1,\text{TP}-}^{\text{DVCS}}\sin(\phi-\phi_S)\sin(\phi)\right]\right\}, \tag{4}$$

$$I = -\frac{K_{\text{I}}e_\ell}{\mathcal{P}_1(\phi)\mathcal{P}_2(\phi)}\left\{\sum_{n=0}^{3} c_{n,\text{unp}}^{\text{I}}\cos(n\phi) + \lambda\left[\sum_{n=1}^{2} s_{n,\text{unp}}^{\text{I}}\sin(n\phi)\right]\right.$$
$$+ S_\perp\left[\sum_{n=0}^{3} c_{n,\text{TP}-}^{\text{I}}\sin(\phi-\phi_S)\cos(n\phi)\right.$$

$$\left. + \sum_{n=1}^{3} s_{n,\text{TP}+}^{\text{I}}\cos(\phi-\phi_S)\sin(n\phi)\right]$$
$$+ \lambda S_\perp\left[\sum_{n=0}^{2} c_{n,\text{TP}+}^{\text{I}}\cos(\phi-\phi_S)\cos(n\phi)\right.$$
$$\left.\left. + \sum_{n=1}^{2} s_{n,\text{TP}-}^{\text{I}}\sin(\phi-\phi_S)\sin(n\phi)\right]\right\}. \tag{5}$$

The symbols $K_{\text{BH}} = 1/[x_B^2 t(1+\varepsilon^2)^2]$, $K_{\text{DVCS}} = 1/(Q^2)$ and $K_{\text{I}} = 1/(x_B y t)$ denote kinematic factors, where $y \equiv (p \cdot q)/(p \cdot k)$ and e_ℓ stands for the (signed) lepton charge in units of the elementary charge. Also, $\lambda = \pm 1$ and $S_\perp$ are respectively the helicity of the lepton beam and the magnitude of the vector $\vec{S}_\perp$, the component of the target polarization vector that is orthogonal to $\vec{q}$. The BH coefficients $c_{n,\text{unp}}^{\text{BH}}$, $c_{n,\text{TP}}^{\text{BH}}$ and $s_{1,\text{TP}}^{\text{BH}}$ in Eq. (3) depend on electromagnetic elastic form factors of the target, while the DVCS (interference) coefficients $c_{n,\text{unp}}^{\text{DVCS}}$ ($c_{n,\text{unp}}^{\text{I}}$), $s_{1,\text{unp}}^{\text{DVCS}}$ ($s_{n,\text{unp}}^{\text{I}}$), $c_{n,\text{TP}+(-)}^{\text{DVCS}}$ ($c_{n,\text{TP}+(-)}^{\text{I}}$) and $s_{n,\text{TP}+(-)}^{\text{DVCS}}$ ($s_{n,\text{TP}+(-)}^{\text{I}}$) involve various GPDs. The squared BH and interference terms in Eqs. (3) and (5) have an additional ϕ dependence in the denominator due to the lepton propagators $\mathcal{P}_1(\phi)$ and $\mathcal{P}_2(\phi)$ [16,26]. The Fourier coefficients appearing in the interference term can be expressed as linear combinations of Compton Form Factors (CFFs) [16], while the coefficients from the squared DVCS term are bilinear in the CFFs. Such CFFs are convolutions of corresponding GPDs with hard scattering coefficient functions.

The coefficients of particular interest in this Letter are $c_{n,\text{TP}}^{\text{BH}}$, $s_{1,\text{TP}}^{\text{BH}}$, $c_{n,\text{TP}+}^{\text{DVCS}}$, $s_{1,\text{TP}-}^{\text{DVCS}}$, $c_{n,\text{TP}+}^{\text{I}}$ and $s_{n,\text{TP}-}^{\text{I}}$, which relate to double-spin asymmetries involving transverse target polarization. The subscript 'TP' is used for BH terms, while the subscript 'TP+' ('TP−') is used for DVCS and interference terms containing $\cos(\phi-\phi_S)$ ($\sin(\phi-\phi_S)$). (The dependences of beam-charge and charge-difference or charge-averaged single-spin asymmetry amplitudes on remaining Fourier coefficients in Eqs. (3)–(5) were discussed in previously published HERMES papers [20–22,24].) The leading-twist (twist-two) coefficients $c_{0,\text{TP}+}^{\text{I}}$, $c_{1,\text{TP}+}^{\text{I}}$ and $s_{1,\text{TP}-}^{\text{I}}$ can be approximated as [16]

$$c_{0,\text{TP}+}^{\text{I}} \simeq \frac{8M_p\sqrt{1-y}K}{Q}y\,\mathcal{R}e\left\{\left(\frac{(2-y)^2}{1-y}+2\right)\mathcal{C}_{\text{TP}+}^{\text{I}} + \Delta\mathcal{C}_{\text{TP}+}^{\text{I}}\right\}, \tag{6}$$

$$c_{1,\text{TP}+}^{\text{I}} \simeq \frac{8M_p\sqrt{1-y}}{Q}y(2-y)\,\mathcal{R}e\,\mathcal{C}_{\text{TP}+}^{\text{I}}, \tag{7}$$

$$s_{1,\text{TP}-}^{\text{I}} \simeq \frac{8M_p\sqrt{1-y}}{Q}y(2-y)\,\mathcal{R}e\,\mathcal{C}_{\text{TP}-}^{\text{I}}. \tag{8}$$

Here, K is a kinematic factor and the C-functions $\mathcal{C}_{\text{TP}+}^{\text{I}}$, $\mathcal{C}_{\text{TP}-}^{\text{I}}$ and $\Delta\mathcal{C}_{\text{TP}+}^{\text{I}}$ can be expressed as linear combination of four CFFs ($\mathcal{H}$, $\mathcal{E}$, $\widetilde{\mathcal{H}}$, and $\widetilde{\mathcal{E}}$) and the Dirac and Pauli electromagnetic form factors F_1 and F_2:

$$\mathcal{C}_{\text{TP}+}^{\text{I}} = (F_1+F_2)\left\{\frac{x_B^2}{2-x_B}\left(\mathcal{H}+\frac{x_B}{2}\mathcal{E}\right) + \frac{x_B t}{4M_p^2}\mathcal{E}\right\}$$
$$- \frac{x_B^2}{2-x_B}F_1\left(\widetilde{\mathcal{H}}+\frac{x_B}{2}\widetilde{\mathcal{E}}\right) + \frac{t}{4M_p^2}\left\{4\frac{1-x_B}{2-x_B}F_2\widetilde{\mathcal{H}}\right.$$
$$\left. - \left(x_B F_1 + \frac{x_B^2}{2-x_B}F_2\right)\widetilde{\mathcal{E}}\right\}, \tag{9}$$

$$\mathcal{C}_{\text{TP}-}^{\text{I}} = \frac{1}{2-x_B}\left(x_B^2 F_1 - (1-x_B)\frac{t}{M_p^2}F_2\right)\mathcal{H}$$

$$+ \left\{ \frac{t}{4M_{\mathrm{p}}^2} \left((2-x_{\mathrm{B}})F_1 + \frac{x_{\mathrm{B}}^2}{2-x_{\mathrm{B}}} F_2 \right) + \frac{x_{\mathrm{B}}^2}{2-x_{\mathrm{B}}} F_1 \right\} \mathcal{E}$$

$$- \frac{x_{\mathrm{B}}^2}{2-x_{\mathrm{B}}} (F_1 + F_2) \left(\widetilde{\mathcal{H}} + \frac{t}{4M_{\mathrm{p}}^2} \widetilde{\mathcal{E}} \right), \tag{10}$$

$$\Delta C_{\mathrm{TP}+}^{\mathrm{I}} = -\frac{t}{M_{\mathrm{p}}^2} \left\{ F_2 \widetilde{\mathcal{H}} - \frac{x_{\mathrm{B}}}{2-x_{\mathrm{B}}} \left(F_1 + \frac{x_{\mathrm{B}}}{2} F_2 \right) \widetilde{\mathcal{E}} \right\}. \tag{11}$$

Note that even if the cross sections were measured for all eight possible combinations of beam charge and helicity and target polarization, at fixed x_{B} and Q^2 it would be impossible to separate the coefficients $c_{n,\mathrm{TP}}^{\mathrm{BH}}$ ($s_{1,\mathrm{TP}}^{\mathrm{BH}}$) and $c_{n,\mathrm{TP}+}^{\mathrm{DVCS}}$ ($s_{1,\mathrm{TP}-}^{\mathrm{DVCS}}$). Nevertheless, the BH coefficients can be calculated from the measured elastic form factors.

2.2. Azimuthal asymmetries

The asymmetries in the cross section for scattering of a longitudinally polarized electron/positron beam off a transversely polarized hydrogen target, which embody the essential features of the Fourier coefficients appearing in Eqs. (3)–(5), can be defined through

$$d\sigma = d\sigma_{\mathrm{UU}}(\phi) \big\{ 1 + e_\ell \mathcal{A}_{\mathrm{C}}(\phi) + \lambda \mathcal{A}_{\mathrm{LU}}^{\mathrm{DVCS}}(\phi) + S_\perp \mathcal{A}_{\mathrm{UT}}^{\mathrm{DVCS}}(\phi, \phi_S)$$

$$+ e_\ell \lambda \mathcal{A}_{\mathrm{LU}}^{\mathrm{I}}(\phi) + e_\ell S_\perp \mathcal{A}_{\mathrm{UT}}^{\mathrm{I}}(\phi, \phi_S) + \lambda S_\perp \mathcal{A}_{\mathrm{LT}}^{\mathrm{BH+DVCS}}(\phi, \phi_S)$$

$$+ e_\ell \lambda S_\perp \mathcal{A}_{\mathrm{LT}}^{\mathrm{I}}(\phi, \phi_S) \big\}, \tag{12}$$

where $d\sigma_{\mathrm{UU}}$ is the cross section for an unpolarized target averaged over both beam charges and both beam helicities. Using the cross sections defined for purely polarized target states ($|S_\perp| = 1$) these asymmetries are expressed as

$$\mathcal{A}_{\mathrm{C}}(\phi) \equiv \frac{1}{8d\sigma_{\mathrm{UU}}} \big[\big(d\vec{\sigma}^{+\uparrow} + d\vec{\sigma}^{+\downarrow} + d\overleftarrow{\sigma}^{+\uparrow} + d\overleftarrow{\sigma}^{+\downarrow} \big)$$

$$- \big(d\vec{\sigma}^{-\uparrow} + d\vec{\sigma}^{-\downarrow} + d\overleftarrow{\sigma}^{-\uparrow} + d\overleftarrow{\sigma}^{-\downarrow} \big) \big], \tag{13}$$

$$\mathcal{A}_{\mathrm{LU}}^{\mathrm{DVCS}}(\phi) \equiv \frac{1}{8d\sigma_{\mathrm{UU}}} \big[\big(d\vec{\sigma}^{+\uparrow} + d\vec{\sigma}^{+\downarrow} - d\overleftarrow{\sigma}^{+\uparrow} - d\overleftarrow{\sigma}^{+\downarrow} \big)$$

$$+ \big(d\vec{\sigma}^{-\uparrow} + d\vec{\sigma}^{-\downarrow} - d\overleftarrow{\sigma}^{-\uparrow} - d\overleftarrow{\sigma}^{-\downarrow} \big) \big], \tag{14}$$

$$\mathcal{A}_{\mathrm{LU}}^{\mathrm{I}}(\phi) \equiv \frac{1}{8d\sigma_{\mathrm{UU}}} \big[\big(d\vec{\sigma}^{+\uparrow} + d\vec{\sigma}^{+\downarrow} - d\overleftarrow{\sigma}^{+\uparrow} - d\overleftarrow{\sigma}^{+\downarrow} \big)$$

$$- \big(d\vec{\sigma}^{-\uparrow} + d\vec{\sigma}^{-\downarrow} - d\overleftarrow{\sigma}^{-\uparrow} - d\overleftarrow{\sigma}^{-\downarrow} \big) \big], \tag{15}$$

$$\mathcal{A}_{\mathrm{UT}}^{\mathrm{DVCS}}(\phi, \phi_S) \equiv \frac{1}{8d\sigma_{\mathrm{UU}}} \big[\big(d\vec{\sigma}^{+\uparrow} - d\vec{\sigma}^{+\downarrow} + d\overleftarrow{\sigma}^{+\uparrow} - d\overleftarrow{\sigma}^{+\downarrow} \big)$$

$$+ \big(d\vec{\sigma}^{-\uparrow} - d\vec{\sigma}^{-\downarrow} + d\overleftarrow{\sigma}^{-\uparrow} - d\overleftarrow{\sigma}^{-\downarrow} \big) \big], \tag{16}$$

$$\mathcal{A}_{\mathrm{UT}}^{\mathrm{I}}(\phi, \phi_S) \equiv \frac{1}{8d\sigma_{\mathrm{UU}}} \big[\big(d\vec{\sigma}^{+\uparrow} - d\vec{\sigma}^{+\downarrow} + d\overleftarrow{\sigma}^{+\uparrow} - d\overleftarrow{\sigma}^{+\downarrow} \big)$$

$$- \big(d\vec{\sigma}^{-\uparrow} - d\vec{\sigma}^{-\downarrow} + d\overleftarrow{\sigma}^{-\uparrow} - d\overleftarrow{\sigma}^{-\downarrow} \big) \big], \tag{17}$$

$$\mathcal{A}_{\mathrm{LT}}^{\mathrm{BH+DVCS}}(\phi, \phi_S) \equiv \frac{1}{8d\sigma_{\mathrm{UU}}} \big[\big(d\vec{\sigma}^{+\uparrow} - d\vec{\sigma}^{+\downarrow} - d\overleftarrow{\sigma}^{+\uparrow} + d\overleftarrow{\sigma}^{+\downarrow} \big)$$

$$+ \big(d\vec{\sigma}^{-\uparrow} - d\vec{\sigma}^{-\downarrow} - d\overleftarrow{\sigma}^{-\uparrow} + d\overleftarrow{\sigma}^{-\downarrow} \big) \big], \tag{18}$$

$$\mathcal{A}_{\mathrm{LT}}^{\mathrm{I}}(\phi, \phi_S) \equiv \frac{1}{8d\sigma_{\mathrm{UU}}} \big[\big(d\vec{\sigma}^{+\uparrow} - d\vec{\sigma}^{+\downarrow} - d\overleftarrow{\sigma}^{+\uparrow} + d\overleftarrow{\sigma}^{+\downarrow} \big)$$

$$- \big(d\vec{\sigma}^{-\uparrow} - d\vec{\sigma}^{-\downarrow} - d\overleftarrow{\sigma}^{-\uparrow} + d\overleftarrow{\sigma}^{-\downarrow} \big) \big], \tag{19}$$

where the symbol $+$ $(-)$ denotes positive (negative) beam charge, $\rightarrow$ $(\leftarrow)$ positive (negative) beam helicity, and $\uparrow$ $(\downarrow)$ the target transverse-polarization direction. The arguments ϕ and ϕ_S are suppressed on the right-hand sides for brevity.

Table 1
The type of the beam particle, the luminosity-averaged beam and target polarizations and the integrated luminosity of the data sets used for the extraction of the various asymmetry amplitudes on a transversely polarized hydrogen target. The data were taken with an e^+ beam during the years 2003 (6.9 pb^{-1}) and 2004 (51.7 pb^{-1}) and an e^- beam during 2005 (98.7 pb^{-1}). The uncertainties for the beam and target polarizations are 2.2% and 8.3%, respectively.

Lepton type	Longitudinal beam polarization (P_ℓ)		Transverse target polarization (S_T)	Luminosity [pb^{-1}]	
	$\leftarrow$	$\rightarrow$		$\leftarrow$	$\rightarrow$
e^-	-0.286	$+0.338$	$+0.721$	29.1	20.1
e^-	-0.286	$+0.338$	-0.721	28.9	20.6
e^+	-0.401	$+0.323$	$+0.721$	11.8	17.5
e^+	-0.401	$+0.323$	-0.721	11.7	17.6
Total				81.5	75.8

3. The HERMES experiment and event selection

The data reported here were collected with the HERMES spectrometer [27] using a longitudinally polarized positron or electron beam of energy 27.6 GeV scattered off a transversely polarized hydrogen gas target internal to the HERA lepton storage ring at DESY. The lepton beam was transversely self polarized by the emission of synchrotron radiation [28]. Longitudinal polarization of the beam at the target was achieved by a pair of spin rotators in front of and behind the experiment [29]. The sign of the beam polarization was reversed approximately every two months. Two Compton backscattering polarimeters [30,31] measured independently the longitudinal and transverse beam polarizations.

The target cell was filled with nuclear-polarized atoms from an atomic beam source based on Stern–Gerlach separation with radio-frequency hyperfine transitions [32]. The nuclear polarization of the atoms was flipped on a time period of 1–3 minutes. The polarization and the atomic fraction of the target gas were continuously monitored [33–35]. The average values of the longitudinal beam polarization P_ℓ and transverse target polarization S_T for the various running periods are given in Table 1. Beam polarization and luminosity are given for the two beam-helicity states separately. The statistical uncertainties of the results reported here are generally larger than those reported in Ref. [24] because here they scale as the inverse of the beam polarization. The target-polarization component S_T is orthogonal to the direction of the incident lepton beam, while $S_\perp$ is orthogonal to the direction of the exchanged virtual photon. This distinction is neglected in this analysis.

The scattered leptons and produced particles were detected by the spectrometer in the polar-angle range 0.04 rad $< \theta <$ 0.22 rad. The average lepton-identification efficiency was at least 98% with hadron contamination of less than 1%.

In this analysis, it was required that events contain exactly one charged-particle track identified as a lepton with the same charge as the beam lepton, and one photon producing an energy deposition $E_\gamma > 5$ GeV in the calorimeter and > 1 MeV in the preshower detector. The following kinematic requirements were imposed on the events, as calculated from the four-momenta of the incoming and outgoing lepton: 1 GeV$^2 < Q^2 < 10$ GeV^2, $W^2 > 9$ GeV^2, $\nu < 22$ GeV and $0.03 < x_{\mathrm{B}} < 0.35$, where $\nu \equiv (p \cdot q)/M_{\mathrm{p}}$ and $W^2 = M_{\mathrm{p}}^2 + 2M_{\mathrm{p}}\nu - Q^2$. The angle between the laboratory three-momenta $\vec{q}$ and $\vec{q}'$ was limited to be less than 45 mrad, and $-t < 0.07$.

An 'exclusive' event sample was selected by requiring the squared missing mass $M_{\mathrm{X}}^2 = (q + p - q')^2$ to be close to the squared proton mass M_{p}^2, with $p = (M_{\mathrm{p}}, 0, 0, 0)$. As the data sample analyzed here is contained in that used in Ref. [24], missing only the

7.5% of that data set recorded in 2002, the M_X^2 distribution is very similar to Fig. 3 of Ref. [24]. The 'exclusive region' for e^+ data is chosen to be $-(1.5)^2$ GeV$^2 < M_X^2 < (1.7)^2$ GeV^2 [36]. This region was shifted by 0.18 GeV^2 for the exclusive events from e^- data. This shift corresponds to the observed difference between the M_X^2 distributions of the e^- and e^+ data samples [24].

4. Extraction formalism

The simultaneous extraction of Fourier amplitudes of beam-charge and target-spin asymmetries combining data collected during various running periods for both beam charges and helicities on a transversely polarized hydrogen target is described in Ref. [24]. It is based on the maximum likelihood technique [37], which provides a bin-free fit in the azimuthal angles ϕ and ϕ_S. In this Letter, almost the same data set is analyzed, omitting the running periods when the beam polarization was small. This analysis differs in that the double-spin asymmetry amplitudes related to the $\mathcal{A}_{LT}$ terms of the cross section given in Eq. (12) are also extracted. Furthermore, eight event weights were employed in the fit to account for luminosity imbalances with respect to beam charge and beam and target polarizations, a technique introduced in Ref. [24].

Based on Eq. (12), the distribution in the expectation value of the yield for scattering of a longitudinally polarized electron/positron beam from a transversely polarized hydrogen target is given by

$$\langle \mathcal{N} \rangle (e_\ell, P_\ell, S_T, \phi, \phi_S)$$
$$= \mathcal{L}(e_\ell, P_\ell, S_T) \eta(\phi, \phi_S) d\sigma_{UU}(\phi)$$
$$\times \left\{ 1 + e_\ell \mathcal{A}_C(\phi) + P_\ell \mathcal{A}_{LU}^{DVCS}(\phi) + S_T \mathcal{A}_{UT}^{DVCS}(\phi, \phi_S) \right.$$
$$+ e_\ell P_\ell \mathcal{A}_{LU}^I(\phi) + e_\ell S_T \mathcal{A}_{UT}^I(\phi, \phi_S)$$
$$\left. + P_\ell S_T \mathcal{A}_{LT}^{BH+DVCS}(\phi, \phi_S) + e_\ell P_\ell S_T \mathcal{A}_{LT}^I(\phi, \phi_S) \right\}, \quad (20)$$

where $\mathcal{L}$ denotes the integrated luminosity and η the detection efficiency. The asymmetries $\mathcal{A}_C$, $\mathcal{A}_{LU}^{DVCS}$, $\mathcal{A}_{UT}^{DVCS}$, $\mathcal{A}_{LU}^I$, $\mathcal{A}_{UT}^I$, $\mathcal{A}_{LT}^{BH+DVCS}$, and $\mathcal{A}_{LT}^I$ are related to the Fourier coefficients in Eqs. (3)–(5) and are expanded in terms of the same harmonics in ϕ and $\phi - \phi_S$ in order to extract azimuthal asymmetry amplitudes in a maximum likelihood fit:

$$\mathcal{A}_C(\phi) \simeq \sum_{n=0}^{3} A_C^{\cos(n\phi)} \cos(n\phi), \quad (21)$$

$$\mathcal{A}_{LU}^{DVCS}(\phi) \simeq A_{LU,DVCS}^{\sin\phi} \sin\phi, \quad (22)$$

$$\mathcal{A}_{LU}^I(\phi) \simeq \sum_{n=1}^{2} A_{LU,I}^{\sin(n\phi)} \sin(n\phi), \quad (23)$$

$$\mathcal{A}_{UT}^{DVCS}(\phi, \phi_S) \simeq \sum_{n=0}^{2} A_{UT,DVCS}^{\sin(\phi-\phi_S)\cos(n\phi)} \sin(\phi-\phi_S)\cos(n\phi)$$
$$+ \sum_{n=1}^{2} A_{UT,DVCS}^{\cos(\phi-\phi_S)\sin(n\phi)} \cos(\phi-\phi_S)\sin(n\phi), \quad (24)$$

$$\mathcal{A}_{UT}^I(\phi, \phi_S) \simeq \sum_{n=0}^{3} A_{UT,I}^{\sin(\phi-\phi_S)\cos(n\phi)} \sin(\phi-\phi_S)\cos(n\phi)$$
$$+ \sum_{n=1}^{3} A_{UT,I}^{\cos(\phi-\phi_S)\sin(n\phi)} \cos(\phi-\phi_S)\sin(n\phi), \quad (25)$$

$$\mathcal{A}_{LT}^I(\phi, \phi_S) \simeq \sum_{n=0}^{2} A_{LT,I}^{\cos(\phi-\phi_S)\cos(n\phi)} \cos(\phi - \phi_S)\cos(n\phi)$$
$$+ \sum_{n=1}^{2} A_{LT,I}^{\sin(\phi-\phi_S)\sin(n\phi)} \sin(\phi - \phi_S)\sin(n\phi), \quad (26)$$

$$\mathcal{A}_{LT}^{BH+DVCS}(\phi, \phi_S) \simeq \sum_{n=0}^{1} A_{LT,BH+DVCS}^{\cos(\phi-\phi_S)\cos(n\phi)} \cos(\phi - \phi_S)\cos(n\phi)$$
$$+ A_{LT,BH+DVCS}^{\sin(\phi-\phi_S)\sin\phi} \sin(\phi - \phi_S)\sin\phi, \quad (27)$$

where the approximation is due to the truncation of the Fourier series.

The amplitudes of beam-charge, beam-helicity and target single-spin asymmetries extracted in this analysis with 27 parameters in the fit were compared with analogous results obtained with fewer parameters using the same Monte Carlo data sample. It was found that they agree with high accuracy.

5. Background corrections and systematic uncertainties

The asymmetry amplitudes are corrected for background contributions from the decays to two photons of semi-inclusive neutral mesons (mainly pions) and of exclusive neutral pions, using the method described in detail in Ref. [24]. After applying this correction, the resulting asymmetry amplitudes are expected to originate from single-photon production leaving the target proton intact as well as the associated production involving excitation of the target proton (see the bottom row in the figures in the result section). Due to the limited resolution in missing mass and without detection of the recoil proton, the contribution of the latter process that falls within the exclusive window remains part of the measured signal.

As the target polarization is involved in all the asymmetries reported here and it was flipped on a time period of 1–3 minutes, the effects of any time dependence of detector efficiencies or acceptance can be safely neglected. The dominant contributions to the total systematic uncertainty are the effects of the limited spectrometer acceptance and from the finite bin widths used for the final presentation of the results. The latter is determined as the difference of the asymmetry amplitudes evaluated from yields integrated over one bin in all kinematic variables, compared to the amplitudes calculated at the average values of the kinematic variables. The combined contribution to the systematic uncertainty from limited spectrometer acceptance, detector smearing, finite bin width, and imperfections in the alignment of the spectrometer elements with respect to the beam is determined from a Monte Carlo simulation using a parameterization [38] of the VGG model [39] (see details in Ref. [24]). In each kinematic bin, the resulting systematic uncertainty is defined as the root-mean-square average of the five differences between the asymmetry amplitude extracted from the Monte Carlo data based on five GPD model variants [38] and the corresponding model predictions calculated analytically at the mean kinematic values of that bin.

Another source of systematic uncertainty comes from the relative shift of the squared missing mass distribution between e^- and e^+ data (see Section 3). One quarter of the difference between the asymmetries extracted with standard and shifted missing-mass windows is assigned for this uncertainty. The background correction also makes a contribution to the uncertainty [24]. There is an additional overall scale uncertainty arising from the uncertainties in the measurement of the beam and target polarizations, which are given in Table 1 and stated in the captions of the figures and tables in the results section. Not included is any contribution due
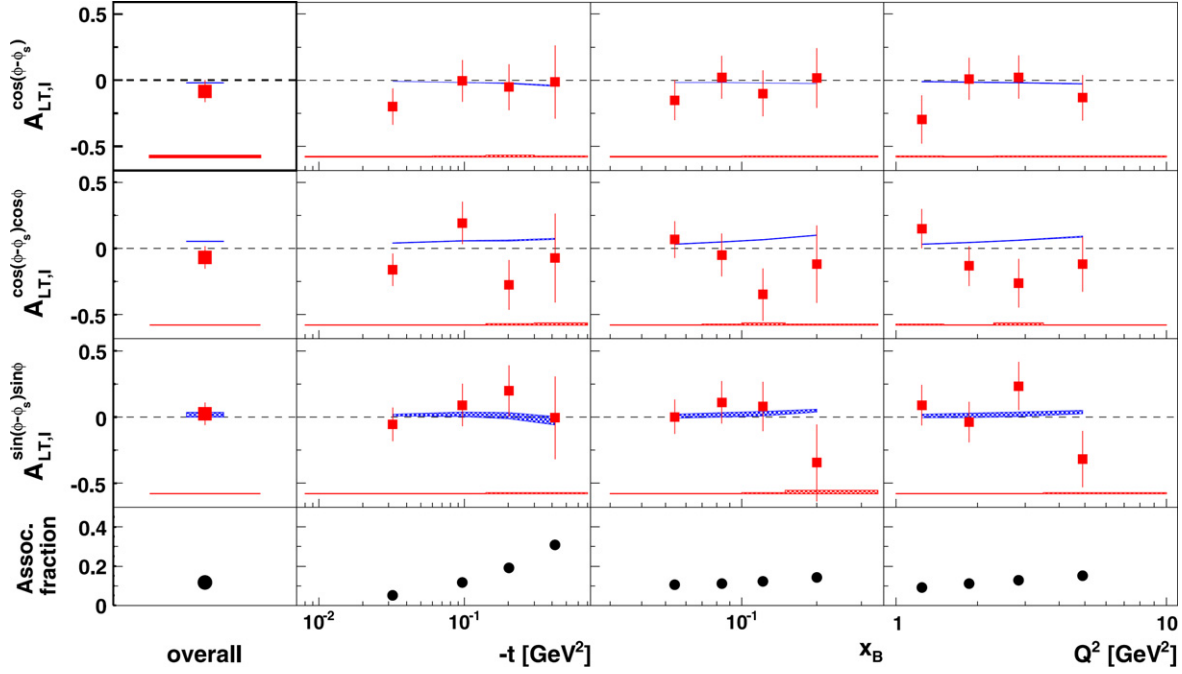
Fig. 2. Charge-difference double-spin asymmetry amplitudes describing the dependence of the interference term on transverse target polarization in combination with beam helicity and beam charge extracted from hydrogen target data. These asymmetry amplitudes correspond to $n = 0$ and $n = 1$ in Eq. (26). The error bars (bands at the bottom of the panels) represent the statistical (systematic) uncertainties. There is an additional overall 8.6% scale uncertainty arising from the uncertainties in the measurements of the beam and target polarizations. The curves show the results of theoretical calculations using the VGG double-distribution model [39,41] with a Regge ansatz for modeling the t dependence of GPDs [42]. The widths of the curves represent the effect of varying the total angular momentum J_u of u-quarks between 0.2 and 0.6, with $J_d = 0$. The bottom row shows the fractional contribution of associated BH production as obtained from a MC simulation.
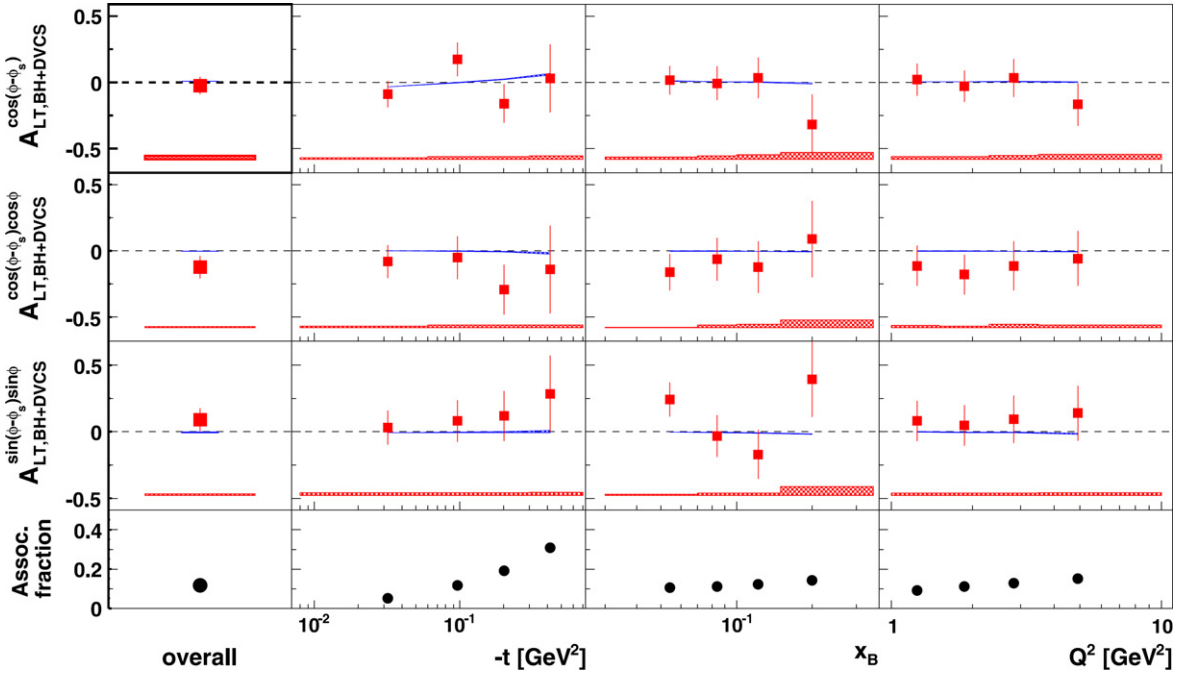

Fig. 3. Charge-averaged double-spin asymmetry amplitudes describing the dependence of the sum of squared DVCS and BH terms on transverse target polarization in combination with beam helicity extracted from hydrogen target data. These asymmetry amplitudes correspond to $n = 0$ and $n = 1$ in Eq. (27). The error bars (bands at the bottom of the panels) represent the statistical (systematic) uncertainties. There is an additional overall 8.6% scale uncertainty arising from the uncertainties in the measurements of the beam and target polarizations. The curves and the bottom row of panels have the same meaning as in Fig. 2.

to additional QED vertices, as for the case of polarized target and polarized beam the most significant of these has been estimated to be negligible [40]. The total systematic uncertainty in a kinematic bin is determined by adding quadratically all contributions to the systematic uncertainty for that bin.

6. Results

All of the asymmetry amplitudes in Eqs. (21)–(27) are extracted simultaneously in a fit to the data. The results for beam-charge, charge-averaged or charge-difference single-spin asymmetry

Table 2
Results for azimuthal Fourier amplitudes of the asymmetry $\mathcal{A}_{LT}^{I}$. An additional 8.6% scale uncertainty is present in the amplitudes due to the uncertainties of the beam and target polarization measurements.

Kinematic bin		$\langle -t \rangle$ [GeV²]	$\langle x_B \rangle$	$\langle Q^2 \rangle$ [GeV²]	$A_{LT,I}^{\cos(\phi-\phi_s)} \pm \delta_{\text{stat}} \pm \delta_{\text{syst}}$	$A_{LT,I}^{\cos(\phi-\phi_s)\cos\phi} \pm \delta_{\text{stat}} \pm \delta_{\text{syst}}$	$A_{LT,I}^{\cos(\phi-\phi_s)\cos(2\phi)} \pm \delta_{\text{stat}} \pm \delta_{\text{syst}}$
Overall		0.12	0.09	2.5	$-0.083 \pm 0.082 \pm 0.008$	$-0.068 \pm 0.083 \pm 0.005$	$0.027 \pm 0.105 \pm 0.005$
$-t$ [GeV²]	0.00–0.06	0.03	0.08	1.9	$-0.199 \pm 0.135 \pm 0.007$	$-0.162 \pm 0.123 \pm 0.006$	$-0.062 \pm 0.169 \pm 0.003$
	0.06–0.14	0.10	0.10	2.5	$-0.004 \pm 0.156 \pm 0.007$	$0.193 \pm 0.158 \pm 0.007$	$0.358 \pm 0.201 \pm 0.012$
	0.14–0.30	0.20	0.11	2.9	$-0.052 \pm 0.173 \pm 0.013$	$-0.275 \pm 0.187 \pm 0.014$	$-0.074 \pm 0.224 \pm 0.006$
	0.30–0.70	0.42	0.12	3.5	$-0.011 \pm 0.274 \pm 0.008$	$-0.071 \pm 0.335 \pm 0.017$	$-0.255 \pm 0.360 \pm 0.020$
x_B	0.03–0.07	0.10	0.05	1.5	$-0.150 \pm 0.150 \pm 0.004$	$0.067 \pm 0.136 \pm 0.005$	$0.137 \pm 0.178 \pm 0.007$
	0.07–0.10	0.10	0.08	2.2	$0.021 \pm 0.162 \pm 0.006$	$-0.049 \pm 0.160 \pm 0.008$	$-0.046 \pm 0.208 \pm 0.005$
	0.10–0.15	0.13	0.12	3.1	$-0.101 \pm 0.171 \pm 0.010$	$-0.348 \pm 0.196 \pm 0.018$	$-0.064 \pm 0.227 \pm 0.007$
	0.15–0.35	0.20	0.20	5.0	$0.017 \pm 0.226 \pm 0.009$	$-0.118 \pm 0.292 \pm 0.010$	$0.240 \pm 0.299 \pm 0.020$
Q^2 [GeV²]	1.0–1.5	0.08	0.06	1.2	$-0.296 \pm 0.182 \pm 0.011$	$0.150 \pm 0.148 \pm 0.008$	$0.221 \pm 0.217 \pm 0.006$
	1.5–2.3	0.10	0.08	1.9	$0.011 \pm 0.157 \pm 0.005$	$-0.131 \pm 0.150 \pm 0.004$	$-0.150 \pm 0.201 \pm 0.006$
	2.3–3.5	0.13	0.11	2.8	$0.022 \pm 0.163 \pm 0.010$	$-0.261 \pm 0.184 \pm 0.017$	$-0.006 \pm 0.212 \pm 0.004$
	3.5–10.0	0.19	0.17	4.9	$-0.132 \pm 0.171 \pm 0.008$	$-0.119 \pm 0.206 \pm 0.005$	$0.138 \pm 0.232 \pm 0.012$

Kinematic bin		$\langle -t \rangle$ [GeV²]	$\langle x_B \rangle$	$\langle Q^2 \rangle$ [GeV²]	$A_{LT,I}^{\sin(\phi-\phi_s)\sin\phi} \pm \delta_{\text{stat}} \pm \delta_{\text{syst}}$	$A_{LT,I}^{\sin(\phi-\phi_s)\sin(2\phi)} \pm \delta_{\text{stat}} \pm \delta_{\text{syst}}$
Overall		0.12	0.09	2.5	$0.026 \pm 0.084 \pm 0.004$	$-0.016 \pm 0.101 \pm 0.005$
$-t$ [GeV²]	0.00–0.06	0.03	0.08	1.9	$-0.053 \pm 0.127 \pm 0.005$	$0.063 \pm 0.164 \pm 0.005$
	0.06–0.14	0.10	0.10	2.5	$0.092 \pm 0.158 \pm 0.005$	$0.069 \pm 0.187 \pm 0.006$
	0.14–0.30	0.20	0.11	2.9	$0.198 \pm 0.193 \pm 0.009$	$-0.200 \pm 0.219 \pm 0.010$
	0.30–0.70	0.42	0.12	3.5	$-0.004 \pm 0.310 \pm 0.010$	$-0.144 \pm 0.324 \pm 0.026$
x_B	0.03–0.07	0.10	0.05	1.4	$0.003 \pm 0.131 \pm 0.006$	$0.135 \pm 0.176 \pm 0.003$
	0.07–0.10	0.10	0.08	2.1	$0.113 \pm 0.158 \pm 0.007$	$-0.209 \pm 0.197 \pm 0.007$
	0.10–0.15	0.13	0.12	3.1	$0.080 \pm 0.186 \pm 0.007$	$-0.074 \pm 0.210 \pm 0.005$
	0.15–0.35	0.20	0.20	5.0	$-0.343 \pm 0.288 \pm 0.025$	$0.028 \pm 0.290 \pm 0.019$
Q^2 [GeV²]	1.0–1.5	0.08	0.06	1.2	$0.092 \pm 0.152 \pm 0.006$	$0.234 \pm 0.215 \pm 0.007$
	1.5–2.3	0.10	0.08	1.9	$-0.037 \pm 0.153 \pm 0.006$	$0.022 \pm 0.185 \pm 0.004$
	2.3–3.5	0.13	0.11	2.8	$0.236 \pm 0.178 \pm 0.007$	$-0.324 \pm 0.210 \pm 0.010$
	3.5–10.0	0.19	0.17	4.9	$-0.316 \pm 0.210 \pm 0.008$	$0.128 \pm 0.220 \pm 0.010$

Table 3
Results for azimuthal Fourier amplitudes of the asymmetry $\mathcal{A}_{LT}^{BH+DVCS}$. An additional 8.6% scale uncertainty is present in the amplitudes due to the uncertainties of the beam and target polarization measurements.

Kinematic bin		$\langle -t \rangle$ [GeV²]	$\langle x_B \rangle$	$\langle Q^2 \rangle$ [GeV²]	$A_{LT,BH+DVCS}^{\cos(\phi-\phi_s)} \pm \delta_{\text{stat}} \pm \delta_{\text{syst}}$	$A_{LT,BH+DVCS}^{\cos(\phi-\phi_s)\cos\phi} \pm \delta_{\text{stat}} \pm \delta_{\text{syst}}$	$A_{LT,BH+DVCS}^{\sin(\phi-\phi_s)\sin\phi} \pm \delta_{\text{stat}} \pm \delta_{\text{syst}}$
Overall		0.12	0.09	2.5	$-0.025 \pm 0.066 \pm 0.025$	$-0.122 \pm 0.083 \pm 0.009$	$0.090 \pm 0.084 \pm 0.012$
$-t$ [GeV²]	0.00–0.06	0.03	0.08	1.9	$-0.088 \pm 0.098 \pm 0.012$	$-0.079 \pm 0.124 \pm 0.014$	$0.032 \pm 0.127 \pm 0.019$
	0.06–0.14	0.10	0.10	2.5	$0.175 \pm 0.126 \pm 0.023$	$-0.050 \pm 0.159 \pm 0.023$	$0.081 \pm 0.158 \pm 0.022$
	0.14–0.30	0.20	0.11	2.9	$-0.160 \pm 0.146 \pm 0.020$	$-0.291 \pm 0.188 \pm 0.023$	$0.119 \pm 0.189 \pm 0.023$
	0.30–0.70	0.42	0.12	3.5	$0.030 \pm 0.256 \pm 0.024$	$-0.138 \pm 0.331 \pm 0.023$	$0.287 \pm 0.287 \pm 0.023$
x_B	0.03–0.07	0.10	0.05	1.5	$0.016 \pm 0.108 \pm 0.017$	$-0.161 \pm 0.135 \pm 0.006$	$0.242 \pm 0.127 \pm 0.010$
	0.07–0.10	0.10	0.08	2.2	$-0.007 \pm 0.126 \pm 0.022$	$-0.064 \pm 0.160 \pm 0.016$	$-0.032 \pm 0.158 \pm 0.015$
	0.10–0.15	0.13	0.12	3.1	$0.036 \pm 0.152 \pm 0.034$	$-0.123 \pm 0.194 \pm 0.026$	$-0.169 \pm 0.183 \pm 0.018$
	0.15–0.35	0.20	0.20	5.0	$-0.315 \pm 0.224 \pm 0.049$	$0.088 \pm 0.287 \pm 0.059$	$0.398 \pm 0.283 \pm 0.067$
Q^2 [GeV²]	1.0–1.5	0.08	0.06	1.2	$0.021 \pm 0.120 \pm 0.021$	$-0.112 \pm 0.149 \pm 0.020$	$0.082 \pm 0.151 \pm 0.018$
	1.5–2.3	0.10	0.08	1.9	$-0.028 \pm 0.120 \pm 0.022$	$-0.179 \pm 0.150 \pm 0.016$	$0.049 \pm 0.152 \pm 0.015$
	2.3–3.5	0.13	0.11	2.8	$0.033 \pm 0.142 \pm 0.030$	$-0.112 \pm 0.185 \pm 0.026$	$0.095 \pm 0.177 \pm 0.018$
	3.5–10.0	0.19	0.17	4.9	$-0.166 \pm 0.159 \pm 0.038$	$-0.057 \pm 0.205 \pm 0.024$	$0.140 \pm 0.205 \pm 0.022$

amplitudes defined in Eqs. (21)–(25) are compatible with those previously published by HERMES [22,24]. They are not considered in this Letter since these amplitudes are here extracted from a subset of previously analyzed data.

The results for the Fourier amplitudes of the *beam-charge-difference* and *charge-averaged* double-spin asymmetries $\mathcal{A}_{LT}^{I}$ and $\mathcal{A}_{LT}^{BH+DVCS}$ defined in Eqs. (26) and (27) are presented in Figs. 2 and 3 respectively, as a function of $-t$, x_B, or Q^2, while integrating over the other variables. (In the HERMES acceptance, x_B and Q^2 are highly correlated.) These values are also given in Tables 2 and 3. The 'overall' results in the left columns correspond to the entire HERMES kinematic acceptance. Fig. 2 shows the leading amplitudes of the double-spin asymmetry related to target trans-

verse polarization combined with beam helicity and beam charge, while Fig. 3 shows the amplitudes of the double-spin asymmetry, which relate to target transverse polarization and beam helicity only. The results for the various harmonics of the asymmetries $\mathcal{A}_{LT}^{I}$ and $\mathcal{A}_{LT}^{BH+DVCS}$ were found to be compatible with zero within the total experimental uncertainties. The bottom row of each figure shows in each kinematic bin the estimated fractional contribution to the yield from associated BH production leading to a baryonic resonant final state. They are obtained from a Monte Carlo simulation using a generator described in Ref. [24]. The two non-leading amplitudes $A_{LT,I}^{\cos(\phi-\phi_S)\cos(2\phi)}$ and $A_{LT,I}^{\sin(\phi-\phi_S)\sin(2\phi)}$ (the case $n = 2$ in Eq. (26)) not shown in Fig. 2 are found to be compatible with zero (see Table 2) within the total experimental uncertainty. The
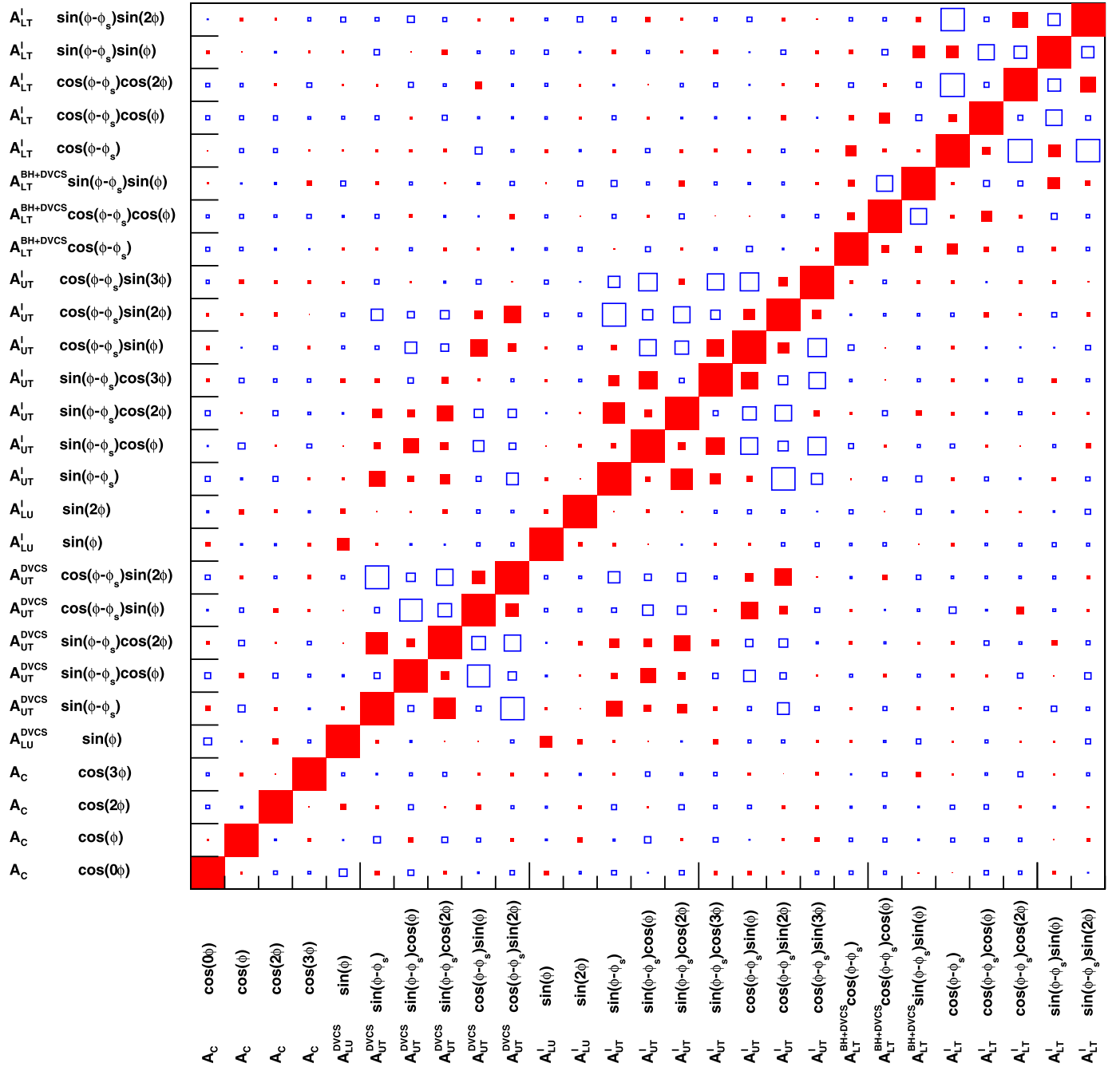
Fig. 4. Correlation matrix for all fitted asymmetry amplitudes. The closed symbols represent positive values, while the open ones are for negative values. The area of the symbols represents the size of the correlation.

correlation among all fitted asymmetry amplitudes is presented in Fig. 4.

The curves in Figs. 2 and 3 represent results of theoretical calculations based on the GPD model described in Ref. [39], using the VGG computer program of Ref. [41]. A Regge ansatz for modeling the t dependence of GPDs [42] is used in these calculations. The model [39] is an implementation of the double-distribution concept [1,2] where the kernel of the double distribution contains a profile function that determines the dependence on ξ, controlled by a parameter b [43] for each quark flavor. The theoretical calculations shown in these figures are obtained for the profile parameters b_{val} and b_{sea} equal to unity and infinity, respectively, which were shown to yield the best agreement with data for the beam-charge asymmetry amplitudes at HERMES [24]. The

leading amplitudes of the target-spin asymmetry $\mathcal{A}_{\text{UT}}^{\text{I}}$ extracted in Ref. [24] have sensitivity to the imaginary parts of the functions $\mathcal{C}_{\text{TP}+}^{\text{I}}$ and $\mathcal{C}_{\text{TP}-}^{\text{I}}$. The latter has significant sensitivity to the CFF $\mathcal{E}$, thereby providing a constraint on the total angular momentum of valence quarks [44,45]. The width of the theoretical curves correspond to variation of the total angular momentum J_u of u-quarks between 0.2 and 0.6, with $J_d = 0$. In principle, the asymmetry amplitude $A_{\text{LT,I}}^{\sin(\phi-\phi_S)\sin\phi}$ could provide a similar constraint through the real part of the function $\mathcal{C}_{\text{TP}-}^{\text{I}}$, as can be seen from Eq. (10). Unfortunately, due to different kinematic prefactors, this amplitude is expected to be suppressed compared to those extracted from the asymmetry $\mathcal{A}_{\text{UT}}^{\text{I}}$, and model calculations also indicate that it is much less sensitive to quark total angular momentum.

7. Summary

Double-spin asymmetries in exclusive electroproduction of real photons from a transversely polarized hydrogen target are measured for the first time with respect to target polarization combined with beam helicity and beam charge, and with respect to target polarization combined with beam helicity alone. The asymmetries arise from the interference between the deeply virtual Compton scattering and Bethe–Heitler processes. The asymmetries are observed in the exclusive region in missing mass that includes the proton together with baryonic resonances. The dependences of these asymmetries on $-t$, x_B, or Q^2 are investigated. The results for various harmonics of the asymmetries $\mathcal{A}_{LT}^{I}$ and $\mathcal{A}_{LT}^{BH+DVCS}$ were found to be compatible with zero within the total experimental uncertainties. Nevertheless, they may serve as additional constraints in global fits to extract GPDs from measurements. The measured asymmetry amplitudes are not incompatible with the predictions of the only available GPD-based calculation.

Acknowledgements

References

[1] D. Müller, et al., Fortschr. Phys. 42 (1994) 101.
[2] A.V. Radyushkin, Phys. Lett. B 380 (1996) 417.
[3] X. Ji, Phys. Rev. Lett. 78 (1997) 610.
[4] J.P. Ralston, B. Pire, Phys. Rev. D 66 (2002) 111501.
[5] M. Burkardt, Phys. Rev. D 62 (2000) 071503;
M. Burkardt, Phys. Rev. D 66 (2002) 119903, Erratum.
[6] M. Diehl, Eur. Phys. J. C 25 (2002) 223;
M. Diehl, Eur. Phys. J. C 31 (2003) 277, Erratum.
[7] A.V. Belitsky, D. Müller, Nucl. Phys. A 711 (2002) 118.
[8] M. Diehl, Phys. Rept. 388 (2003) 41.
[9] A.V. Belitsky, A.V. Radyushkin, Phys. Rept. 418 (2005) 1.
[10] J. Blümlein, B. Geyer, D. Robaschik, Nucl. Phys. B 560 (1999) 283.
[11] A.V. Belitsky, D. Müller, Nucl. Phys. B 537 (1999) 397.
[12] A.V. Belitsky, A. Freund, D. Müller, Nucl. Phys. B 574 (2000) 347.
[13] A.V. Belitsky, D. Müller, Phys. Lett. B 486 (2000) 369.
[14] I.V. Anikin, O.V. Teryaev, Phys. Rev. D 76 (2007) 056007.
[15] K. Kumerički, D. Müller, K. Passek-Kumerički, Eur. Phys. J. C 58 (2008) 193.
[16] A.V. Belitsky, D. Müller, A. Kirchner, Nucl. Phys. B 629 (2002) 323.
[17] CLAS Collaboration, S. Stepanyan, et al., Phys. Rev. Lett. 87 (2001) 182002.
[18] CLAS Collaboration, F.X. Girod, et al., Phys. Rev. Lett. 100 (2008) 162002.
[19] CLAS Collaboration, G. Gavalian, et al., Phys. Rev. C 80 (2009) 035206.
[20] HERMES Collaboration, A. Airapetian, et al., Phys. Rev. Lett. 87 (2001) 182001.
[21] HERMES Collaboration, A. Airapetian, et al., Phys. Rev. D 75 (2007) 011103.
[22] HERMES Collaboration, A. Airapetian, et al., JHEP 0911 (2009) 083.
[23] JLAB Hall A Collaboration, C.M. Camacho, et al., Phys. Rev. Lett. 97 (2006) 262002.
[24] HERMES Collaboration, A. Airapetian, et al., JHEP 0806 (2008) 066.
[25] A. Bacchetta, U. D'Alesio, M. Diehl, C.A. Miller, Phys. Rev. D 70 (2004) 117504.
[26] M. Diehl, T. Gousset, B. Pire, J.P. Ralston, Phys. Lett. B 411 (1997) 193.
[27] HERMES Collaboration, K. Ackerstaff, et al., Nucl. Instr. and Meth. A 417 (1998) 230.
[28] A. Sokolov, I. Ternov, Sov. Phys. Doklady 8 (1964) 1203.
[29] J. Buon, K. Steffen, Nucl. Instr. and Meth. A 245 (1986) 248.
[30] D.P. Barber, et al., Nucl. Instr. and Meth. A 338 (1994) 166.
[31] M. Beckmann, et al., Nucl. Instr. and Meth. A 479 (2002) 334.
[32] A. Nass, et al., Nucl. Instr. and Meth. A 505 (2003) 633.
[33] C. Baumgarten, et al., Nucl. Instr. and Meth. A 496 (2003) 606.
[34] C. Baumgarten, et al., Nucl. Instr. and Meth. A 508 (2003) 268.
[35] HERMES Collaboration, A. Airapetian, et al., Nucl. Instr. and Meth. A 540 (2005) 68.
[36] F. Ellinghaus, Ph.D. thesis, Humboldt Universität zu Berlin, Germany, January 2004, DESY-THESIS-2004-005.
[37] R. Barlow, Nucl. Instr. and Meth. A 297 (1990) 496.
[38] V.A. Korotkov, W.D. Nowak, Eur. Phys. J. C 23 (2002) 455.
[39] M. Vanderhaeghen, P.A.M. Guichon, M. Guidal, Phys. Rev. D 60 (1999) 094017.
[40] A.V. Afanasev, M.I. Konchatnij, N.P. Merenkov, J. Exp. Theor. Phys. 102 (2006) 220.
[41] M. Vanderhaeghen, P.A.M. Guichon, M. Guidal, Computer code for the calculation of DVCS and BH processes in the reaction $ep \to ep\gamma$, private communication, 2007.
[42] K. Goeke, M.V. Polyakov, M. Vanderhaeghen, Prog. Part. Nucl. Phys. 47 (2001) 401.
[43] L.V. Musatov, A.V. Radyushkin, Phys. Rev. D 61 (2000) 074027.
[44] F. Ellinghaus, W.D. Nowak, A.V. Vinnikov, Z. Ye, Eur. Phys. J. C 46 (2006) 729.
[45] QCDSF-UKQCD Collaboration, D. Brommel, et al., PoS LATTICE 2007 (2007) 158.